Photon counting arrays for AO wavefront sensors

John Vallerga[*a], Anton Tremsin[a], Jason McPhate[a], Bettina Mikulec[b], Allan Clark[b] and Oswald Siegmund[a]
[a]Space Sciences Laboratory, 7 Gauss Way, Univ. of California, Berkeley, CA USA 94720-7450;
[b]University of Geneva, 24, quai Ernest-Ansermet, 1211 Geneva 4, Switzerland

ABSTRACT

Future wavefront sensors for AO on large telescopes will require a large number of pixels and must operate at high frame rates. Unfortunately for CCDs, there is a readout noise penalty for operating faster, and this noise can add up rather quickly when considering the number of pixels required for the extended shape of a sodium laser guide star observed with a large telescope. Imaging photon counting detectors have zero readout noise and many pixels, but have suffered in the past with low QE at the longer wavelengths (> 500 nm). Recent developments in GaAs photocathode technology, CMOS ASIC readouts and FPGA processing electronics have resulted in noiseless WFS detector designs that are competitive with silicon array detectors, though at ~ 40% the QE of CCDs. We review noiseless array detectors and compare their centroiding performance with CCDs using the best available characteristics of each. We show that for sub-aperture binning of 6x6 and greater that noiseless detectors have a smaller centroid error at fluences of 60 photons or less, though the specific number is dependent on seeing conditions and the centroid algorithm used. We then present the status of a 256x256 noiseless MCP/Medipix2 hybrid detector being developed for AO.

Keywords: : adaptive optics, wavefront sensors, MCP, Medipix, GaAs photocathodes

1. INTRODUCTION

As adaptive optic (AO) systems grow more complex and faster to support the next generation of large telescopes, the demands on the wavefront sensor(s) (WFS) must increase as well. Achieving concurrently the large number of phase measurements (~5000) at ~kHz frame rates[1] is a key technological challenge for the WFS detector of all types (Shack Hartmann, pyramid, curvature etc[2].).

The detector of choice for most array-based wavefront sensor detectors are silicon charge coupled devices (CCDs), which have high QE in the optical. In a CCD, the charge generated by the photon flux at each pixel is transferred to a high gain, low noise amplifier to create an analog voltage for digitization. The noise associated with this amplification increases at faster clocking rates. Given the standard readout schemes of clocking the detected charge through a finite number of on-chip amplifiers, there is a direct tradeoff between the number of pixels readout per second and the readout noise per pixel. This puts pressure on AO system designers to decrease the number of pixels used per phase measurement (e.g., the Quad cell for Shack Hartmann sensors) and/or to slow down the frame rate. Recent efforts to improve CCD readouts include: completely parallel readouts with one amplifier per column[3] which allows a slower clock rate for a given frame rate; gain stages in the serial readout structure that amplify the charge signal before the signal is sensed by the readout amplifier (L3CCD by E2V technologies[4]) which reduces the effective readout noise; and clever geometrical pixel layout structures that match the multiple regions of interest, thereby simultaneously reducing the number of pixels and increasing the number of parallel readout amplifiers.[5]

Alternatives to charge integrating arrays are photon counting detectors. “Photon counting” detectors are so named because photon events are detected and counted individually. The detectors are considered “noiseless” in that the readout of N events (whole number) implies that N events were detected. This is not to say that the next measurement of the same phenomena will be N events, that is governed by the statistics of the photon arrival (“photon noise”). It is the readout noise of photon counters that is zero. [Often, the background event rate in photon counting detectors due to cosmic rays, scattered light and thermionic emission are referred to as “noise” or “dark noise” but the detection and counting of those events are real measurements and the term “noiseless” hereafter in this paper refers strictly to the readout noise.]

*jvv@ssl.berkeley.edu; phone 1 510 643 5666

Astronomical Adaptive Optics Systems and Applications II, edited by Robert K. Tyson, Michael Lloyd-Hart,
Proceedings of SPIE Vol. 5903, 59030M, (2005) · 0277-786X/05/$15 · doi: 10.1117/12.620295

Photon counting imaging detectors not only count the event but also provide the x,y position of each event and sometime the time, t, of each event. Examples in the UV and optical include avalanche photodiode (APDs) arrays[6] and imaging MCP detectors[7]. Silicon based APDs are fast and potentially have the high QE of silicon in the optical and near IR but are not yet incorporated in large arrays. Imaging microchannel plate (MCP) detectors can have large area (100 x 100 mm), high spatial resolution (20 μm FWHM), low background dark count, and event timing resolution less than 1 nanosec[7]. Their QE is determined by the characteristics of the photocathode material that absorbs the initial photon and releases the photoelectron.

So why haven't photon counting arrays taken over the field of WFS detectors given their lack of readout noise? Simply stated, the optical quantum efficiency has been too low compared to CCDs. Whereas CCDs with QE > 80% are quite common, image tubes with typical semitransparent photocathodes might barely achieve ~ 15% QE at 600nm. This QE ratio is such that it does not take much photon fluence for the signal to noise ratio of CCDs to exceed the signal to noise ratio of photon counting detectors, where the noise in this case is the inherent photon noise of the input flux. Recently, there has been much progress in producing high optical QE photocathodes, resulting from the development of Generation III night vision devices. The QE of these photocathodes is now exceeding 50%, in particular for GaAs and GaAsP[8] (Fig. 1).

Given this improvement, we explore the capabilities of photon counting arrays for WFS detectors. We first describe many different types of noiseless photon counting detectors and compare their characteristics to the requirements of future large telescope wavefront sensors. We then discuss in detail the advantages of large area noiseless detectors for WFS and compare them with existing state of the art, high QE CCDs. We then present a progress report on the development of the optical Medipix detector, a 256x256 photon counting array consisting of an MCP image tube with a specialized CMOS ASIC readout called the Medipix2[9,10]

2. PHOTON COUNTING ARRAY DETECTORS

A photon counting array detector can detect a single photon without ambiguity, enabling the downstream electronics to increment some sort of counter in a histogram, either spatial, spectral or temporal. In the UV/optical regime, photon interactions with matter usually result in a single photoelectron that is difficult to detect directly with simple linear amplifiers. If this single photoelectron can be amplified before external measurement, such that the resulting number of electrons significantly exceeds the downstream amplifier noise, then the amplifier output can be used to count the photons directly. If the gain, G, of this amplification process is constant and independent of the number of input photoelectrons, then the internal amplifier is said to be proportional (or linear), i.e. the output amplifier pulse is proportional to the input number of photons. If the gain is *not* constant from pulse to pulse, the output signal has an excess noise due to the amplification process itself.

If the gain mechanism can saturate, such that any size input (except zero) results in the same output amplitude, the amplifier is said to be in "Geiger" mode, where all information of the input number of events for that pulse is lost except that it was equal to or greater than 1 event. There is no "excess noise" because the amplitude of the event is not used, just the existence of the event itself. However, if the Geiger mode detector can recover fast enough such that the probability of 2 events occurring in this time is very low, then simply counting the Geiger mode events in an integration time gives the detected input flux. It is this mode that is usually referred to as photon counting, where each event is temporally distinct.

A penalty for photon counting is the associated deadtime per event when either the input transducer (photon to photoelectron to amplified pulse) or downstream counting electronics are busy and cannot process another event. The deadtime per event varies with detector, and can range from 10ns to 10μs. For random and uncorrelated input flux (e.g. starlight) a deadtime of a microsecond would correspond to a 10% deadtime for a 100kHz average input rate, i.e. 10% of the input photons would not be detected. This loss can be completely characterized, calibrated and corrected, but it is equivalent to a rate dependent QE loss. Therefore to operate at high detector input flux, many independent parallel channels must be used. Counting each photon allows arbitrary integration times, which can be very fast, dependent only on the speed and dynamic range of the counter. However, for high rate parallel counter systems, the speed of the counter readout must also be factored into the integration time. The time it would take to readout all the counters in a 2D array would represent an effective minimum frame time.

2.1 Single photon avalanche diode arrays (SPADs)

Single photon APDs[11] are silicon diodes biased above their breakdown voltage thereby operating in the Geiger mode. A photo-generated electron can instigate a breakdown in the high electric field region of the diode leading to a

large current pulse. The diode is biased through a current limiting resistor which reduces the bias voltage below the breakdown regime, thus self limiting the event in time and amplitude. They can be fabricated using CMOS technology widely used in the microelectronics industry. By miniaturizing the APDs to small spatial pixels (20 μm), many performance characteristics can all be reduced such as: bias voltages (~30V), afterpulsing, deadtime (70ns) and dark rate (200Hz at 25C). Thin active regions limit APD QE to 30% at 650nm (14) that could be increased at the expense of timing resolution.

Existing problems with SPAD arrays include optical and electrical cross talk between pixels, requiring finite physical separation leading to low fill factors on the input surface (3%). Use of a Shack-Hartmann type WFS would then require another lenslet array attached to the detector to focus the light onto the sensitive element. Cryogenic cooling can reduce dark count rate. Designs are also being discussed[12] to back-thin planar arrays and create a 3D drift region to focus the photoelectrons to the high field breakdown area. This would increase the fill factor and QE, though it has yet to be fabricated.

Silicon APDs hold the promise of high QE photon counters. Yet significant hurdles remain in developing working large arrays (>256x256) that are efficient, do not suffer from crosstalk or afterpulsing, and have reasonable fill factor.

2.2 L3CCDs

A recent new CCD technology is the "Low Light Level" CCD (L3CCD)[4] by E2V Technologies. It uses a special serial shift register that amplifies the pixel charge at every pixel transfer *before* the output preamp, resulting in output gains of up to 1000 e^- per input photon, easily overwhelming the few electron readout noise of the amplifier. Unfortunately, this amplification process in the shift register is not a noiseless process, and at the higher gains, the variance of the signal charge doubles[13]. So to achieve the same shot noise limited signal to noise ratio, you would have to collect twice the number of photons. Also, for the larger CCDs (E2V 97 512x512) the maximum readout rate is 10MHz corresponding to 40 frames/sec. Improving this frame rate might be possible by increasing the number of parallel readout, though each serial amplification register takes up a finite amount of silicon real estate. In the discussions below, the L3CCD technology can be classified as a zero readout noise device with a QE approximately half of its nominal value when using a centroid estimator.

2.3 Imaging, photon counting MCP detectors

The workhorse of space UV astronomy, MCP detectors use a photocathode to convert the photon to a photoelectron that is then amplified in the microchannel(s) and detected by a position sensitive anode. Optical astronomy has been reluctant to adopt this technology because of the lower quantum efficiency of previously available optical photocathodes compared to bulk silicon. The key issue to apply this detector to AO work is to achieve high quantum efficiency, which is now possible through recent developments of GaAs type photocathodes. (Fig. 1). The resultant detector QE is the product of this photocathode QE and the MCP sensitivity to photoelectrons, usually the open-area ratio of the microchannels on the plate (~70%). This would result in detector QE of ~ 35%

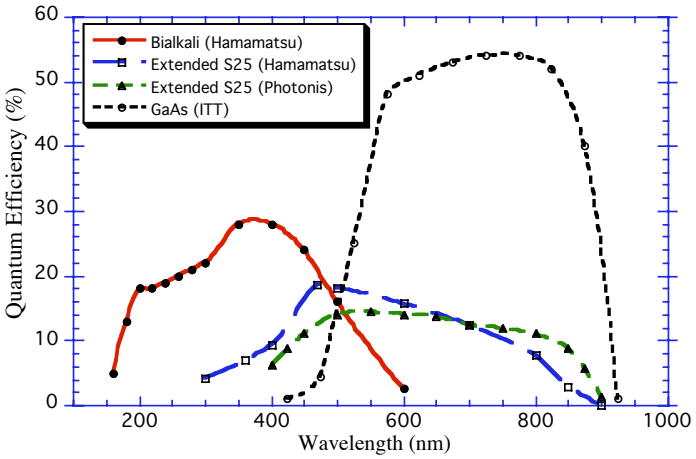

Fig. 1. Quantum efficiencies for commonly used optical regime photocathodes (Sources: www.ittnv.com, www.hamamatsu.com), and the more recent GaAs advances[11].

Electronic MCP readout anodes use either time delay[14] or charge centroiding[15] to determine the event location. Both the x,y position as well at the time of arrival can be transmitted for every event. Spatial resolutions of 7 μm FWHM and timing resolution of 100 ps have been demonstrated, and detectors of 100x100 mm are possible[7,14,15].The problem with these styles of readout is they are inherently serial in nature: one event comes out at a time (x,y,t). That is not a problem in low-light astronomy but for a Shack-Hartmann WFS with 1000 lenslets operating at 1 kHz and imaging 1000 events per spot, the readout event rate required is 1 GHz. To avoid a significant deadtime at

this input rate, a single event would have to be read out in 100 ps (amplification, discrimination, conversion, calculation and resetting) which is a factor of ~ 1000 faster than current capabilities.

To overcome this speed limitation for AO WFS, a massively parallel MCP readout must be used, where each pixel becomes a counter. The photons are still being counted, but the counts (not charge like a CCD) are being integrated at the pixel level. The counters are then read out on a frame basis after an integration period. The individual photon arrival time is sacrificed in this mode, but the array still has zero readout noise. Also, as digital numbers, the counters can be read out very fast.

2.4 MCP/Medipix2 hybrid detector

We have been developing a new hybrid detector that can achieve a kHz frame rate with noiseless readout and still achieve a QE in the optical of 35%. (Details of this detector design can be found in reference 10.) The detector (Fig. 2) is a microchannel plate (MCP) image tube with a GaAs photocathode and a new pixelated CMOS readout chip called the "Medipix2". Photons interacting with the photocathode release a photoelectron that is proximity focused to the MCP input face. The MCP amplifies this single photoelectron with a gain on the order of 10^4. The resultant charge cloud exits the MCP and lands on the input pad of a Medipix2 pixel where it is counted as one event. The pixel counter will integrate until it is read out in a digital, noiseless process. Also, because the data is digital, it can be read out at ~246 MHz pixel rates, which corresponds to a frame readout time of 286 µs for the current Medipix2 chip.

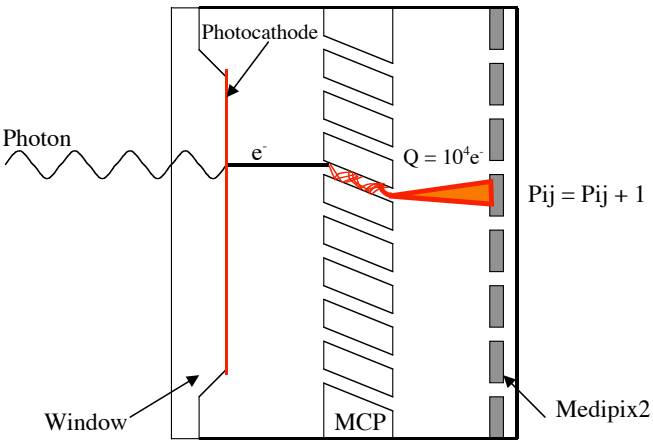

Fig. 2. Schematic of a sealed microchannel plate image sensor. A single photon results in a single count in the pixel Pij. Our scheme uses the Medipix2 ASIC as the readout.

The Medipix2 chip is a pixel detector readout chip consisting of 256 x 256 identical elements, each working in a single photon counting mode. Each pixel consists of a preamplifier, a discriminator, and a 14 bit pseudo-random counter. The counter logic, based on a shift register, also behaves as the input/output register for the pixel. It was designed and manufactured in a six-metal 0.25µm CMOS technology. Each 55 x 55 µm pixel contains ~500 transistors. The total active area of the chip is 1.98 cm^2 and is 3-side buttable to support larger arrays.

Typical cathodes (semitransparent) for the optical such as bialkali, and multi-alkali are somewhat difficult to produce and require ultrahigh vacuum ($<10^{-8}$ Torr). The best multi-alkali S20 and S25 photocathodes (semitransparent) produced have ~10% to 15% QE at 600 nm (Fig. 1) which is not adequate for AO applications. GaAs photocathodes have been used extensively for a number of years, mainly in night vision applications as the photocathode for Generation III image intensifiers. During that time many advances in performance have been achieved. As demonstrated in Fig. 1, quantum efficiencies in excess of 50% can now be achieved from 550nm to 850nm making them very attractive for astronomical applications.

A vacuum demountable detector with MCPs and a Medipix2 readout have been used to test many aspects of the new detector. We are now working with a commercial vendor to incorporate the MCPs and Medipix2 into a vacuum tube with a GaAs type photocathode. Reference 16 details the tube design efforts to date. We expect the first working tubes to be available in the fall of 2005.

3. WAVEFRONT SENSOR PERFORMANCE WITH PHOTON COUNTING DETECTORS

There are many techniques for measuring the wavefront phase, its slope, or its curvature across a pupil. Most use 2 dimensional detector arrays to detect a flux distribution. The optimization of the readout detector is usually quite similar: maximize photon detection efficiency, minimize readout nose and background while reading out fast enough to meet the required loop bandwidth characteristics of the AO system and sky turbulence. As telescopes get larger, the number of actuators of the deformable mirror are increasing, placing new demands on larger detector formats as well.

We will use the Shack-Hartmann WFS as a convenient model to calculate improvements gained from a noiseless detector, but we expect these improvments to be applicable to the other styles of WFS.

The Shack-Hartmann WFS measures the centroid location of an array of spots focused by a lenslet array in th epupil plane. Most image the individual sub-pupils sampled by the lenslet array onto a 2x2 pixel subarray (the "quad cell"), and use a normalized difference algorithm to measure the centroid of the spot which represents the slope of the wavefront, e.g. x_{cent} = (A-B)/(A+B). However, if the input spot illumination has a width on the order of a pixel, then the measured centroid of the input vs. its true centroid is not a linear function of the true position. Furthermore, as the illumination input changes width, the slope of the relationship between measured and true centroid changes. This slope is related to the gain of the feedback to the actuators. So in variable seeing conditions, where the spot sizes are changing, poor phase control can result. If more pixels are applied to the measurement, this "undersampling distortion" can be substantially reduced.

If the pixels are made smaller in order to properly sample the spot distribution, then smaller arrays can suffer from truncation where a fraction of the spot falls outside the NxN array. Fig. 3 shows a comparison of the measured centroids versus their true input position for a 4x4 and a 6x6 pixel cell sampling array for 5 different spots sizes. It is clear that in the 4x4 case, the slope of the gain function is a strong function of the spot size, while the added pixels of the 6x6 case give a tighter distribution on the gain slopes.

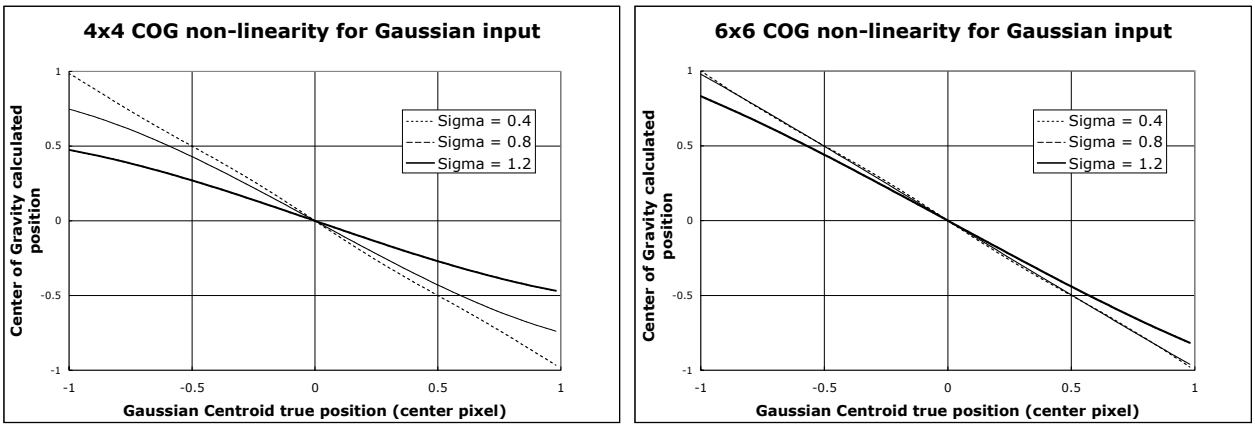

Fig. 3. Model of measured centroid vs. true centroid using pixellated sampling of a Gaussian input function in one dimension. The plotted curves represent different rms widths of the Gaussian input as a fraction of pixel size and the centroid algorithm is a "center of gravity" type where x_{cent} is the sum of the pixel values weighted by the pixel number and divided by the sum of the pixel values. In all cases the signal to noise ratio was infinite. The slope of the 4x4 cell algorithm curves change dramatically with input width while the 6x6 algorithm slopes are similar for different input widths. Most of the non-linearity for the larger input functions is due to truncation error where the signal falls off the edge of the NxN array.

Besides the robustness of the centroid determination to spot size, another reason to add more pixels (NxN) to the determination of the centroid is the freedom to operate the WFS "off null". The reference (null) position of the centroid does not have to reside at the center of a quad array. If the spatial response is linear, the null position can be anywhere in the NxN array (except of course, too near the edge where truncation effects occur). This makes it much easier to match the WFS plate scale and offset to the detector array. Also, for large telescopes, the laser guide star image is not at the same focus as the science object due to the finite height of the laser scatter from the atmosphere. Keeping the telescope focused on the science object requires keeping the LGS spots slightly off-null. In theory, if the number of pixels per spot is large enough, the WFS can be operated "open-loop" and put outside the control loop.

A third reason for having more pixels per pupil element is the parallax to the LGS image for larger telescopes. Using a Na laser guide star, a ~10 km thick Na layer observed with a 30 meter telescope will have the return images stretched to ~ 3" in the radial direction. If the pixel size matches the seeing at a good site, then 6x6 or 8x8 pixels is required to keep all the photons on the WFS detector subpupil array.

There is no error penalty in the centroid determination using more pixels with a noiseless detector. This is not the case with a detector with readout noise. The centroid error (in radians) of a standard center of gravity calculation for a detector with readout noise scales as N^2 (for an NxN array of pixels)[17]. For a large number of pixels, there are better ways to calculate the spot centroid such as Gaussian weighting[17], correlation[18], thresholding and windowing[19]. These techniques reduce the centroid error by strongly weighting pixels with higher SNR and weakly weighting the pixels that

are mostly noise. These "matched filter" algorithms can also help with noiseless detectors, improving the centroid error in the photon noise limit as well. For both types of detector, more pixels take longer to readout and calculate the centroid, and a smaller number of spots will be measured with a fixed number of total detector pixels.

To illustrate the advantage of noiseless detectors when the number of pixels per subpupil image increases and the flux is limited, we have modeled a Gaussian distributed stellar image onto an NxN pixel array and varied the input fluence and the pixel size (Fig. 4). Four cases have been compared corresponding to the four columns of Fig. 4. The leftmost column represents an 8x8 sampling of the (centered) stellar image with a noiseless detector assuming a QE of 35%, similar to what we expect the performance of the MCP/Medipix2 tube. The 3 columns to the right represent a CCD with a QE of 90% and a readout noise of 2.5e$^-$ rms but different pixels sizes over the same field of view (FOV): 8x8, 6x6 and 4x4. The greyscale of each image has been stretched from the minimum to the maximum signal level per pixel and each image was a separate run of the random Monte Carlo code generating the input photon locations. At the fluence of 1000 photons, all four produce an obvious centroid, though the number of events in the CCD are higher and

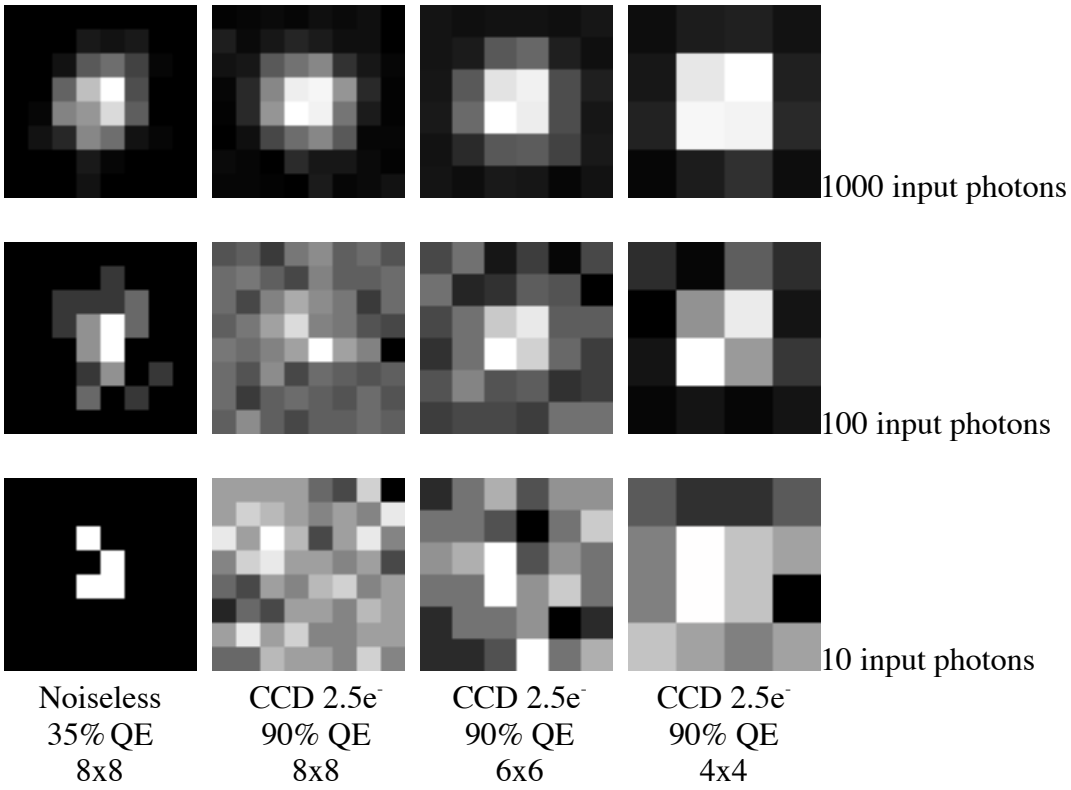

Figure 4. Model simulation of Shack Hartmann spots imaged with detectors of different QE, noise and pixel size. In each case the FOV remains the same and the star image is centered with the same size in all cases with respect to the FOV (2.5 pixels in the 8x8 format case). The top row assumes 1000 incident photons, the middle 100 and the bottom 10 photons. The first column is a noiseless detector sampled by 8x8 pixels, and the three columns on the right assume a 2.5e- rms readout noise and a QE of 90%, but with different pixel sampling. Note how the readout noise masks the smaller signal in the lower rows while for the noiseless detector a centroid is easily determined, though less accurate than the higher fluence cases.

analytically have a smaller error on the measured centroid (see below). For the 100 photon fluence, the noise of the CCD images becomes more obvious, especially for the 8x8 and 6x6 cases. When the fluence is only 10 photons, a reasonable centroid is only possible with the ~4 detected events in the noiseless detector. So even with a QE handicap of a factor of 2.57, the noiseless detector is superior at the lowest light levels.

3.1 Centroid error comparison of noiseless detectors with CCDs

It is clear that a noiseless detector's centroid determination using more pixels can be more accurate and linear. But that is only true if the QE is the same for both detectors, which currently it is not. When the lower QE of a photon

counting detector is factored in, the number of actual detected events is lower and even though the contribution of readout noise is zero, the SNR of the just photon Poisson noise is less for the lower QE detector. At high fluence levels where the noise is dominated by the photon arrival statistics, the higher QE detector will always win by the ratio of the QEs to the one half power. At very low flux levels, the winner depends strongly on the number of pixels and the centroiding algorithm used.

To see quantitatively where this crossover point exists between a photon counting detector and a charge integrating CCD, we have adopted the weighted centroid of gravity (WCOG) phase difference error formulas of Fusco et al.[17]:

$$(\sigma^2_{\Delta\phi})_{ph} = \frac{\pi^2}{2\ln(2)(N_{ph})} \bullet \left(\frac{N_T}{N_D}\right)^2 \bullet \left(\frac{N_T^2 + N_W^2}{2N_T^2 + N_W^2}\right)^2$$

$$(\sigma^2_{\Delta\phi})_{\det} = \frac{\pi^3}{32(\ln(2))^2} \bullet \left(\frac{\sigma_{det}}{(N_{ph})}\right)^2 \bullet \left(\frac{N_T^2 + N_W^2}{N_D}\right)^2$$

$$(\sigma^2_{\Delta\phi})_{tot} = (\sigma^2_{\Delta\phi})_{det} + (\sigma^2_{\Delta\phi})_{ph}$$

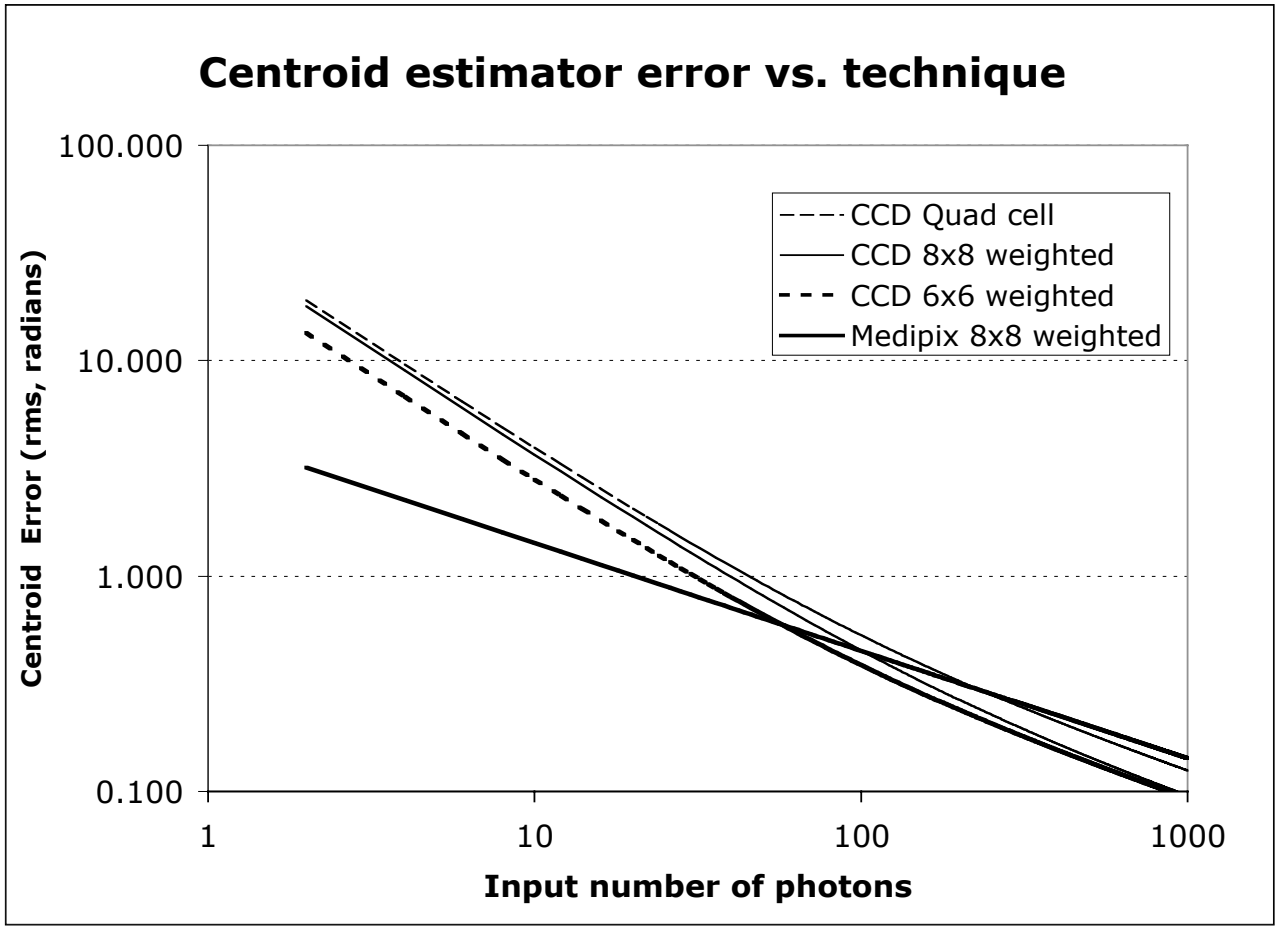

Fig. 5. Plot of resultant rms phase difference (in radians) due to centroid error using different detectors and centroiding algorithms. Plotted is a noiseless detector using an 8x8 pixel array ("Medipix 8x8") to sample a 3 pixel FWHM Gaussian distributed spot. The other three lines are for a 90% QE CCD with 2.5e- rms readout noise sampling the same star spot using a 8x8, 6x6 and quad cell format. In all cases besides the quad cell, the weighted center of gravity centroid algorithm[17] was used to determine the centroid error

where $(\sigma^2_{\Delta\phi})_{tot}$ is the total phase difference error variance across a subaperture, $(\sigma^2_{\Delta\phi})_{ph}$ and $(\sigma^2_{\Delta\phi})_{det}$ are the phase error variances for the photon and detector readout noise respectively, and σ_{det} is the readout noise in electrons (= 0 for noiseless detector). N_{ph} is the number of *detected* input photons and is a function of the QE of the detector. These formula use a Gaussian weighting function where the free parameter is the width of the weighting Gaussian (N_w, FWHM in pixels) used to multiply the assumed Gaussian stellar input distribution. The first two formula represent the centroid error variance due to photon noise and readout noise respectively, and are added directly before taking the square root to determine the rms centroid error. The other two parameters, N_T and N_D are the size of the stellar distribution (FWHM in pixels) and the size of the diffraction limited PSF, (FWHM, in pixels) respectively. N_T and N_D can differ in bad seeing conditions, with $N_T > N_D$. Details on the derivation of these formulae are given in reference 17.

To make this comparison timely, we have adopted detector QE and noise parameters of two state of the art devices: a 264x264 pnCCD that can be read out at 1kHz frame rate with 2.5 e- noise and a QE of 90%[3] and the 256x256 pixel MCP/Medipix2 tube (discussed above) with published GaAs QE at 600 nm multiplied by a 70% open area ratio of MCPs resulting in a predicted 35% QE. The different data sets in the plot represent different centroiding techniques for the CCD: 8x8 pixel, 6x6 pixel, and quad cell. The pixel size changes in each such that the field of view of the NxN array is $4\lambda/d$, where λ is the wavelength and d is the subaperture size. The 8x8 Medipix plot assumes zero readout noise. All data sets use the weighted center of gravity algorithm except the quad cell. The stellar width, N_T is set 50% larger that the diffraction limit, N_D, which is 2 pixels for the 8x8 case, 1.5 pixels for 6x6 and 0.5 pixel for 2x2. The weighting function width is set equal to the stellar width ($N_T = N_W$). So in all cases the stellar width and diffraction width stay the same (in angle), the only change is the size and number of pixels per image.

The first thing to notice in Fig. 5 is that the noiseless detector is better than the CCDs at low fluence levels in determining a centroid and therefore a phase slope. Even with a QE ratio of 2.5, not until the fluence reaches 60 input photons does the CCD (6x6 weighted) match the Medipix/MCP/GaAs tube. The phase difference error (rms) across the subaperture for the noiseless Medipix tube is 1.0 radian at 20 input photons and 0.58 radians at 60 input photons. This corresponds to a phase error of $\lambda/6$ and $\lambda/11$ respectively for this sampling and seeing conditions. The second thing to notice is how good the weighted center of gravity algorithm is compare to a simple quad cell formula. This result is not new and many have proposed various weighting schemes to enhance low SNR data[17,18,19].

For the CCD, the 6x6 binning is better than the 8x8, because the light is concentrated on a smaller number of noisy pixels. 4x4 sampling would even have been slightly better. But we decided not to show this data as we believe the trend is towards more pixels per Shack-Hartmann spot and all the advantages such an approach offers in linearity and operational flexibility.

4. STATUS OF THE MCP/MEDIPIX2 HYBRID DETECTOR AND LINEARITY RESULTS

The major components of the MCP/Medipix2 hybrid detector optical tube all exist and work well separately. Combining them into one vacuum tube is a technological challenge due to the nature of vacuum tube processing. We have demonstrated that the MCPs and the Medipix work well together in laboratory vacuums[10]. GaAs photocathodes are regularly produced for night vision tubes and have been incorporated in other hybrid detector schemes where they have achieved excellent QE of greater than 50%[8]. Our efforts over the last year have concentrated on the design and construction of the piece parts of a standard 18mm MCP vacuum tube including a special ceramic and metal header that the Medipix2 chip is glued to and routes the ~60 signal pins through hermetic feedthroughs outside the vacuum. We are at the point where we have to demonstrate the survival of the Medipix2 chip to the elevated (~250 to 325 C) vacuum tube processing temperatures necessary to maintain the cleanliness and vacuum stability required for a GaAs photocathode. Similar CMOS chips have survived such processing[20] and we are confident that the Medipix2 will as well. Details on our efforts and mechanical tube design can be found in reference 16.

4.1 Linearity and centroid error with simulated Shack-Hartmann test

MCPs and the Medipix2 ASICs have their own unique sampling formats. The individual pores that make up MCPs are arranged in a hexagonal format with an open area ratio of ~ 70% to collect the photoelectrons. The Medipix2 ASIC 55 μm square pixel has an 18 μm width octagon input pad on its top surface, which samples the MCP output charge cloud. The MCP pore spacing of 12 μm is small compared to the Medipix pixels, but we were not sure whether sub-pixel centroiding would reveal unexpected effects such as Moiré beating and other fixed pattern distortions. We therefore attempted to mimic a Shack-Hartmann WFS detector input and measure its ability to determine centroids across a pixel. To simulate such a situation, we used an image mask (an electroformed Ni sheet with a 10 μm diameter

pinhole array at 500 μm spacing in both directions) between a movable light source, a UV pen-ray lamp with 2 mm aperture, and the detector. The mask was fixed about 2.5 mm above the input MCP (chevron stack, 10 μm pores on 12 μm centers), and the lamp was at about 50 cm distance. There were approximately 700 spots produced on the detector in a grid that was slightly rotated relative to the Medipix2 readout pixels (see Fig. 6). The spot widths are determined mostly by the diffraction of the UV light through the small pinholes. The missing spots in the pinhole array image are due to blocked pinholes on the mask and there are a few dead columns in the ASIC readout.

Data was acquired with an MCP gain of about 60 ke per detected photon and 1600 V rear field to keep the lateral extent of the charge cloud exiting the MCPs small. The 25 s integration time resulted in about 600 photons per spot. Each data run consisted of two integrations taken at each of 11 lamp locations on 2 mm increments from 0 to 20 mm and aimed at investigating the spot movement. The x and y locations of each spot were found by fitting a Gaussian to the x and y profiles of a 9 x 9 pixel area surrounding each spot. For each lamp offset, the location of each spot was compared to its location in the first image (the 0 mm lamp position) and the x- and y-shifts calculated for each spot and

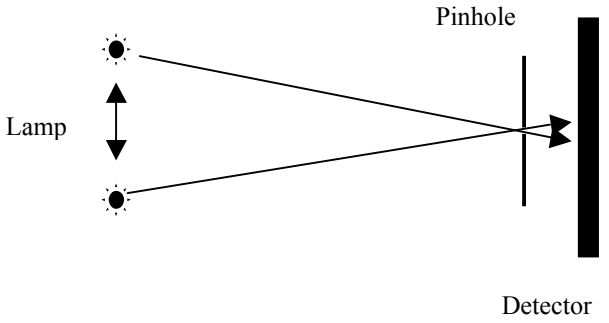

Figure 6. Linearity test setup. A pinhole mask was placed above the MCP/Medipix detector and illuminated with UV light (above). The pinholes are 10μm diameter and spaced at 500 μm intervals. The UV light diffracted through the pinhole array creating the image to the right with approx. 600 events per spot. This spot array was translated across the detector by moving the lamp. At each lamp position, the centroids of each spot were determined and compared to the reference image (lamp position zero, see next figure.). Some pinholes are blocked and there are a few dead columns on the readout ASIC.

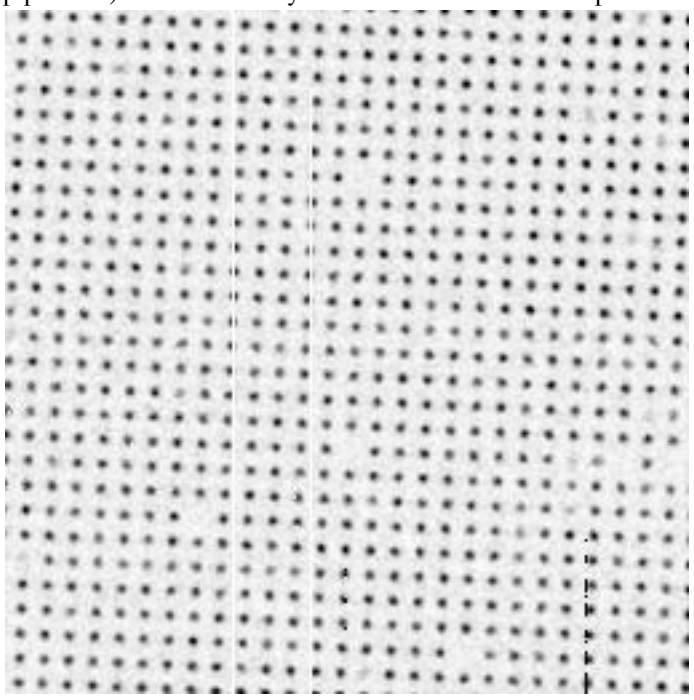

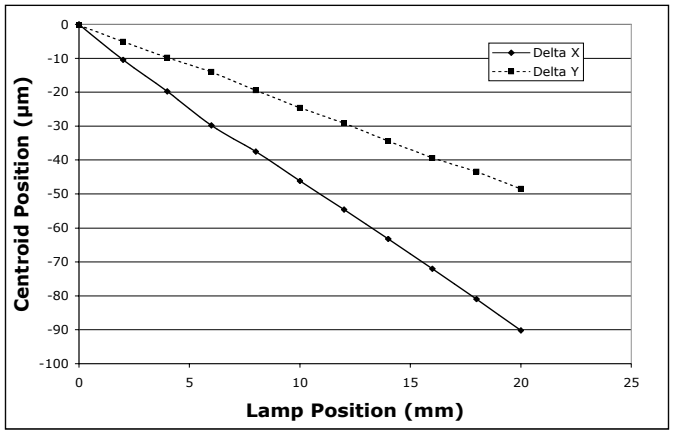

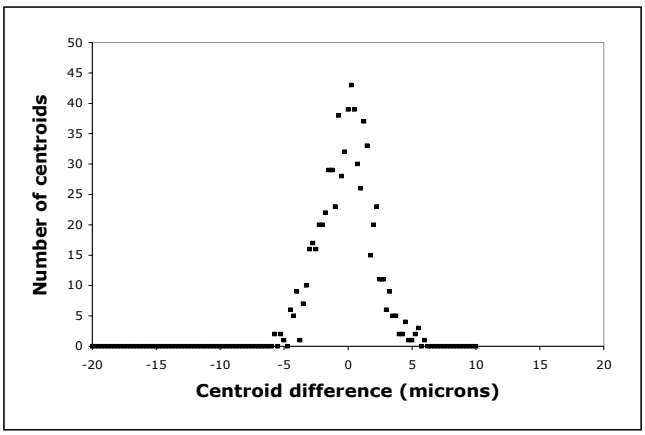

Figure 7. One the left is the average centroid position versus lamp position for the setup shown in Figure 6. As the lamp is moved in a linear fashion at an arbitrary angle with respect to the pinhole grid, the average centroid positions shift in a similar fashion across the detector. On the right is a distribution of centroid differences (minus the expected shift). The standard deviation of this distribution is approx. 2.5 microns, consistent with the size of the spots and the number of events in each spot.

averaged. The result is plotted in Fig. 7 and shows the good linear response of the detector in both directions even across pixel boundaries. (The slopes are different as the lamp moved an arbitrary angle with respect to the pinhole grid axes.)

A histogram of the distribution of the centroid differences of two lamp positions is shown in Fig. 7. Because the spacing of the pinhole array is not a multiple of the 55μm pixel spacing, the 700 pinholes represent a uniform sample of subpixel input locations and non-linearities in the sub-pixel centroid calculation would appear to widen this distribution. The distribution rms is ~2.5 μm compared to the expected rms of 2.9 μm expected for a 600 event spot with a 3 pixel FWHM. This clearly demonstrates the sub-pixel linearity of the MCP/Medipix2 hybrid.

5. SUMMARY AND CONCLUSIONS.

This paper presented the case for noiseless optical detectors for wavefront sensing in adaptive optics. Their use would allow the application of more pixels per sub-aperture phase measurement, increasing the linearity and therefore the robustness of each measurement, especially off-null and non-symmetric extended spot distributions. Even with QEs of only 35%, noiseless detectors still have an advantage over CCDs with 2.5e- rms readout noise for fluences less than ~60 photons using weighted center of gravity centroid estimators, though the details of the exact crossover fluence are a strong function of seeing conditions and specific centroid estimator, bin size and FOV. For a quad cell, the crossover point is ~ 200 photons. This advantage at low flux levels allows the use of dimmer natural guide stars and/or shorter exposures, both being desirable. If the goal, however, is to derive and control to the lowest phase error (i.e., extreme AO), then in the limit of very high fluence, it always makes sense to use the detector with the highest QE.

What is new now is that noiseless array detectors are being developed with QEs approaching (~factors of 2 to 3) that of CCDs. Each new promising technology has certain advantages and specific weaknesses to overcome. In this paper we concentrated on the MCP/Medipix2 hybrid optical vacuum tube we are developing. If the Medipix2 ASIC can be successfully integrated into a vacuum tube while maintaining the high QE of a GaAs photocathode, then the performance modeled above will come available to AO system designers who can then design WFS with detectors that have high pixel count, operate at high frame rates and have zero readout noise.

ACKNOWLEDGMENTS

The authors wish to thank the Medipix Collaboration for the Medipix2 chips, readout hardware and software and for valuable advice. This material presented here is based upon work supported by AURA through the NSF under AURA cooperative agreement # AST-0132798-SPO#6(AST-0336888)

REFERENCES

1. Angel, R. et al “A Roadmap for the Development of Astronomical Adaptive Optics “, July 6, 2000, available at http://www.noao.edu/dir/ao/
2. R. K Tyson, ”Introduction to Adaptive Optics”, SPIE Press, Bellingham, Washington, USA, 2000.
3. R. Hartmann, H. Gorke, N. Meidinger, H. Soltau, L. Strüder, “Results of a fast pnCCD detector system”, SPIE, 5903, 2005 (this conference)
4. Mackay C. D., Tubbs R. N., Bell R., Burt D. J., Jerram P., Moody I., “Subelectron read noise at MHz pixel rates”, SPIE, 4306, 298, 2001
5. Beletic, James W., "Follow the yellow-orange rabbit: a CCD optimized for wavefront sensing a pulsed sodium laser guide star", SPIE, 5499, pp. 302 - 309, 2004
6. A. Rochas, A. Pauchard, O. Guinnard, L. Monat, and A. Matteo,” CMOS-based SinglePhoton Detectors and Potential Applications”, NIM-A, 2005 (in press)
7. Siegmund O. H. W., “Advances in microchannel plate detectors for UV/visible astronomy”, SPIE, 4854, 190, 2003
8. M. Hayashida, R. Mirzoyan, and M. Teshima, “Developement of HPDs with an 18 mm diameter GaAsP photocathode for the MagicII”, in Fourth International Conference on New developments in photodetection Beaune, France, 19-24 June 2005 NIM-A, 2005 (in press)
9. Llopart X. and M. Campbell, “First test measurements of a 64k pixel readout chip working in single photon counting mode” Nuclear Instruments and Methods in Physics Research Section A: Volume 509, Issues 1-3, 21 August 2003 ,Pages 157-163

10. Vallerga, John V., McPhate, Jason, Mikulec, Bettina, Tremsin, Anton, Clark, Allan, and Siegmund, Oswald, "Noiseless imaging detector for adaptive optics with kHz frame rates", SPIE, 5490, pp. 1256 - 1267, 2004
11. Zappa, Franco, Tisa, Simone, Cova, Sergio, Maccagnani, Piera, Bonaccini Calia, Domenico, Bonanno, Giovanni, Belluso, Massimiliano, Saletti, Roberto, and Roncella, Roberto, "Pushing technologies: single-photon avalanche diode arrays", SPIE, 5490, pp. 1200 - 1210, 2004
12. Gerhard Lutz, P. Holl, M. Laatiaoui, C. Merck, H.G. Moser, N. Otte, R.H. Richter, L. Strüder N. Otte, R.H. Richter, and L. Strüde, "Development of Avalanche-Drift and Avalanche-Pixel Detectors for Single Photon Detection and Imaging in the Optical Regime", in Fourth International Conference on New developments in photodetection Beaune, France, 19-24 June 2005 NIM-A, 2005 (in press)
13. Tulloch, Simon M., "Application of L3 technology to wavefront sensing", SPIE, 5490, pp. 1167 - 1176, 2004
14. Siegmund O. H., Gummin M. A., Sasseen T., Jelinsky P. N., Gaines G. A., Hull J., Stock J. M., Edgar M. L., Welsh B. Y., Jelinsky S. R., Vallerga J. V., Microchannel plates for the UVCS and SUMER instruments on the SOHO satellite, SPIE, 2518, 355, 1995
15. Siegmund, O.~H.~W., Tremsin, A.~S., Vallerga, J.~V., Abiad, R., and Hull, J., "High resolution cross strip anodes for photon counting detectors", NIMPA, 504, pp. 177 - 181, 2003
16. J. B. McPhate, J. V. Vallerga, A. S. Tremsin, O. H. Siegmund, B. Mikulec, and A. G. Clark, "A noiseless kilohertz frame rate imaging detector based on microchannel plates readout with the Medipix2 CMOS pixel chip", SPIE, 2005 (in press)
17. Fusco, Thierry, Nicolle, Magalie, Rousset, Gerard, Michau, Vincent, Beuzit, Jean-Luc, and Mouillet, David, "Optimization of a Shack-Hartmann-based wavefront sensor for XAO systems", SPIE, 5490, pp. 1155 - 1166, 2004
18. Poyneer, Lisa A., "Scene-based Shack-Hartmann wave-front sensing: analysis and simulation", ApOpt, 42, pp. 5807 - 5815, 2003
19. Thomas, Sandrine, "Optimized centroid computing in a Shack-Hartmann sensor", SPIE, 5490, pp. 1238 - 1246, 2004
20. Thierry Gys , "Production of 500 Pixel Hybrid Photon Detectors for the RICH counters of LHCb",in Fourth International Conference on new developments in photodetection Beaune, France, 19-24 June 2005 NIM-A, 2005 (in press)